Hindawi
Advances in Civil Engineering
Volume 2021, Article ID 1505482, 13 pages
https://doi.org/10.1155/2021/1505482

Research Article

Numerical Analysis of Bearing Behavior of the Prebored Precast Pile with an Enlarged Base

Zao Ling,[1,2] **Jiangbin Wu**,[3] **and Weidong Wang**[3]

[1]*Guangzhou Municipal Construction Group Co., Ltd., Guangzhou 510030, China*
[2]*School of Civil Engineering, Guangzhou University, Guangzhou 510006, China*
[3]*Underground Space & Engineering Design & Research Institute, East China Architecture Design & Research Institute Co., Ltd., Shanghai 200002, China*

Correspondence should be addressed to Zao Ling; lingzao7000@hotmail.com

Received 28 June 2021; Accepted 19 August 2021; Published 30 August 2021

Academic Editor: Jian Zhang

Prebored precast pile with an enlarged base (PPEB pile) is a new type of green and environmental protection pile foundation developed in China in recent years, which has complex bearing characteristics and many influencing factors. Based on the static load tests and key parameters' tests in deep soft soil in Shanghai, a three-dimensional numerical analysis model was established using ABAQUS finite element software. The transfer law of load among the precast pile, cement soil, and soil around the pile and the action mechanism of the enlarged base were analyzed emphatically, and a sensitivity analysis of the main factors affecting the bearing performance was carried out. The calculation results show that the existence of the enlarged base can greatly improve the compressive bearing capacity, increasing the diameter and height of the enlarged base is beneficial to the bearing capacity, and the influence of the diameter expansion ratio is more effective. With the increase of the proportion of nodular piles, the ultimate bearing capacity increases slightly, but the deformation increases obviously. Under the condition of cement soil of the test piles, the spacing of the neighboring nodules of nodular piles has no obvious effect on the bearing capacity, and the 1 m spacing commonly used in engineering applications can be optimized. The increase of cement soil thickness is beneficial to the improvement of pile bearing capacity, but the efficiency is low. Finally, some improvement measures for the construction technology of the PPEB pile were put forward.

1. Introduction

Prebored precast pile with enlarged base (PPEB pile) is a new type of green and environmental protection pile foundation developed in China in recent years [1]. This PPEB pile requires a special installation process [2], as shown in Figure 1. First, a special mixing drill is used to drill, stir, and grout the soil to form a borehole with an enlarged base filled with cement soil slurry. Then, the precast concrete pile is inserted into the cement soil slurry by its self-weight. After cement soil solidification, the pile structure is composed of rigid pile body wrapped by cement soil. The properties of the cement grout used in the pile shaft and the enlarged base are different. Generally, the premade base-forming cement grout with a water/cement (w/c) ratio of 0.6 is injected into the enlarged base, and side-forming cement grout with a w/c ratio of 1.0 is injected into the borehole. Therefore, the pile body will be in the form of cement soil with low strength around the precast pile and cement soil with high strength at the enlarged base. The inner concrete precast piles can be made up of prestressed high-strength concrete (PHC) piles, PHC nodular piles, prestressed reinforced high-strength concrete (PRHC) piles, and so on.

Due to the special construction technology and complex material composition and structure, the bearing characteristics of the PPEB pile are complex and the influencing factors are numerous. On the basis of static load test and model test, many researchers [2–6] preliminarily discussed the load transfer law of the pile under vertical compression and verified its reliable bearing capacity. It should be emphasized that the number of on-site test piles or models is limited, which makes the analysis results have some limitations. Numerical simulation is an

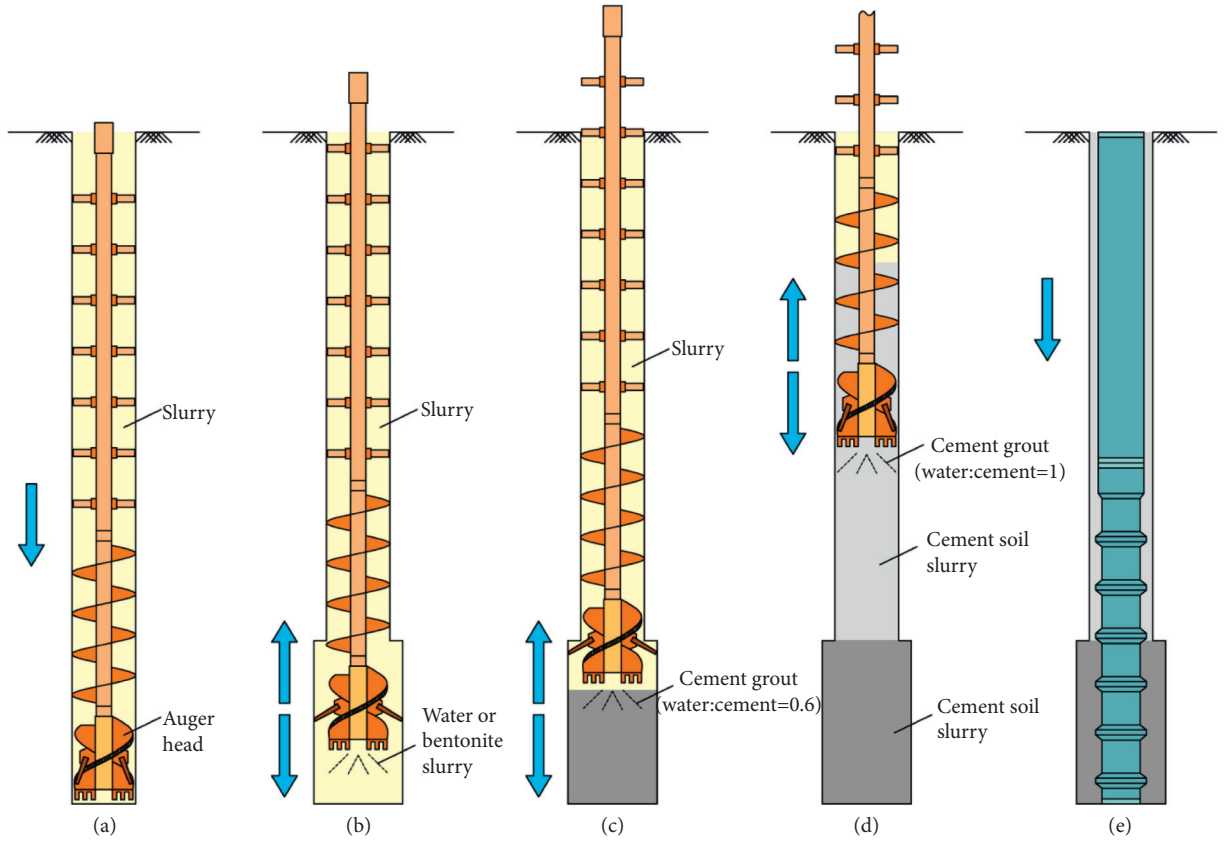

Figure 1: Typical construction sequence of a PPEB pile. (a) Drilling. (b) Expanding base. (c) Grouting at the enlarged base. (d) Grouting along the pile shaft. (e) Inserting the precast pile (modified from [2]).

effective tool for analyzing complex engineering problems, especially the pile-soil interaction. Through numerical analysis, Ye et al. [7–9] discussed load transfer law and the effect of reinforced core on the performance and failure behavior of stiffened deep cement mixing piles. Based on the engineering application of PPEB pile technology in Zhejiang Province, China, Yang et al. [10], Zhou et al. [11], and Xie et al. [12] used the numerical simulation method to analyze the influence of structure size of precast pile, soil properties, cement soil characteristics, and other factors on bearing capacity, which enriched the understanding of the characteristics of PPEB piles. However, the previous numerical research lacks the analysis of the internal stress behavior of pile foundation, which is essential to understand the law of load transfer.

Through field tests in Shanghai, the authors preliminarily discussed the bearing behavior of PPEB piles in deep soft soil stratum [2]. In this paper, based on the above static load tests and key parameter tests, the load transfer law between precast pile, cement soil, and soil around pile and the action mechanism of enlarged base were further analyzed by numerical simulation. Then, a sensitivity analysis of the main factors affecting the compressive bearing performance was carried out.

2. Field Test

The field tests in this paper were carried out in the intersection of Jiang Yang South Road and Hong Wan Road of Shanghai. In general, there are eight soil layers within the upper 70 m of soil below the ground surface. The basic physical and mechanical properties of the soils are shown in Table 1. The effective cohesion and friction angle were determined from consolidated undrained tests. The undrained shear strength was obtained from in situ vane shear tests and empirical values.

Three test piles, designated piles TP1, TP2, and TP3, were installed at the site. The length and shaft diameter of the test piles were 55 m and 750 mm, respectively. The inner precast concrete piles were assembled by a 40 m long, 600 mm diameter PHC pile with 110 mm wall thickness in the upper part and a 15 m long, 650 mm (500 mm) diameter nodular pile (i.e., 500 mm pile shaft diameter, which increases to 650 mm at the nodules) with 100 mm wall thickness in the lower part. The enlarged bases were 2750 mm long with a diameter of 1200 mm. To ensure the material strength of the precast piles, the test piles adopted C100 high-performance concrete with 100 mm cube compressive strength of 120.9 MPa and elastic modulus of 54.7 GPa.

Static load tests were carried out 43–45 days after pile installation. The maintained load method was adopted in accordance with the Chinese code JGJ106-2014 [13]. The test apparatus mainly consisted of a counterforce device using concrete blocks, a loading device using a hydraulic Jack, and a measuring system using force and displacement sensors. The test piles were instrumented with vibrating-wire strain gauges to obtain the axial force of the pile.

Table 1: Summary of soil properties.

Soil layer	Depth (m)	w (%)	γ (kN/m^3)	c' (kPa)	φ' (°)	s_u(kPa)	E_s (MPa)	q_s (kPa)
① Fill	0.0–3.0	25.0	17.0	—	25.0	20	—	—
② Silty clay with silt	3.0–7.0	31.0	18.5	5	32.0	52	10.0	40
③ Soft organic clay	7.0–19.5	50.4	16.7	4	26.7	31	3.3	28
④ Silty clay	19.5–39.5	32.9	18.2	3	30.7	68	5.0	56
⑤ Silty clay with silt	39.5–46.5	23.1	19.7	10	29.6	120	10.5	99
⑥ Silty clay	46.5–51.0	31.0	18.4	7	28.0	113	5.5	89
⑦ Silt mixed silty clay	51.0–59.5	28.2	18.7	2	32.5	178	9.0	89
⑧ Silty sand	59.5–70.0	25.9	19.0	—	35.0	—	12.8	—

w: water content; γ: unit weight; c': effective cohesion; φ': effective friction angle; s_u: undrained shear strength; E_s: compression modulus; q_s: ultimate shaft resistance obtained from the field test.

Obvious inflections can be observed on the load-displacement curves of TP1 and TP2. The displacements were small during the initial stages of loading and increased dramatically when reaching the ultimate bearing capacity of 8800 kN. As the pile head of TP3 was inclined during the test, the load test on TP3 was terminated at the applied load of 8000 kN. The load-displacement curve of TP3 had no obvious inflection. The displacements and applied loads of pile heads at several critical stages are summarized in Table 2. Detailed test results were described in a previous paper [2].

3. Finite Element Numerical Simulation

3.1. Numerical Modeling. Three-dimensional finite element analysis (FEA) method incorporated in the software ABAQUS was used to model the load of TP1. As the vertical loading of a single pile was axisymmetric, half of the model was taken for analysis to simplify the calculation. To minimize the influence of the FEA model boundary, the radius of soil around the pile was 20 m, a width more than 20 times the pile diameter in the plane, and the depth was 80 m, as shown in Figure 2. The distance from the pile toe to the bottom of the entire soil model was more than 20 times the pile diameter to ensure that the boundary effect was negligible. The bottom of the soil model was fixed in all three directions, and the other sides were constrained to allow vertical displacement only. The linear elastic model was used for precast pile and the Mohr–Coulomb elastic-plastic model was used for cement soil and soil around the PPEB pile.

The initial ground stress of the soil was considered in the model, while the displacement control method was used to apply the vertical load. The parameters of the soil were selected according to Table 1. According to the engineering experience in Shanghai [14] and the results of trial calculation, the elastic modulus (E) of soil can be taken as 5 times the compression modulus (E_s). Through the back analysis of the results of the static load test [2], the elastic modulus of the precast pile was 60 GPa and Poisson's ratio was 0.15.

Cement soil is an important part of PPEB pile. The characteristics and parameters of cement soil, precast pile-cement soil interface, and cement soil-soil interface are essential to obtain the correct numerical analysis results. The above parameters related to cement soil would be obtained through comprehensive analysis of field tests and laboratory tests.

3.2. Field and Laboratory Tests of Cement Soil. Consistent with the requirements of the pile hole in the field test, the cement soil mixing pile K1 without precast pile was constructed. It could be considered that the cement soil property of K1 was the same as that of the test piles. Therefore, the core samples were obtained from the K1 for testing. After 48 days of curing, the unconfined compressive strength (*UCS*) of cement soil was 1.7~4.0 MPa, the cohesion was 342~731 kPa, and the internal friction angle was 37~45°. The deformation parameters of cement soil are usually measured by the deformation modulus (E_{50} is the secant modulus of cement soil at 50% compressive strength) [15]. Based on the stress-strain relationship of unconfined compression specimens, the deformation modulus E_{50} of cement soil was estimated to be 102~222 MPa.

Due to the difficulty in drilling construction, the cement soil at the enlarged base could not be sampled and tested. Therefore, according to the composition of the actual enlarged base, the laboratory proportioning tests of cement soil were carried out. The typical silty clay and silty sand in Shanghai were selected as the soil materials, and P·O 42.5 Portland cement was selected as cementitious material. In the actual construction, the amount of cement grout at the pile toe was 100% of the enlarged base volume, and then the drill pipe was stirred up and down evenly for 1 to 5 times. After the completion of grouting, the volume ratio (cement grout/slurry) was about 1.0 to 1.5. In the laboratory test, the specific gravity of the slurry was 1.5, while the water-cement ratio of cement grout was 0.6. The volume ratio (cement grout/slurry) was set to 1, 1.5, and 2 to prepare the cement soil slurry of enlarged base. The rough samples were made by the hanging bag method (see Figure 3) and then cut into cylinders with a height of 100 mm and a diameter of 50 mm.

After 28 days of curing in the standard curing room, the unconfined compressive strength test and shear test were carried out with the loading speed of 1 mm/min. The laboratory test results are shown in Table 3. According to the field and laboratory test results, in the FEA model, the values of cement soil parameters are shown in Table 4. The Poisson's ratios were assumed upon the empirical values.

3.3. Interface Definition. In this FEA model, three interface elements were defined: precast pile-cement soil interface, precast pile-soil interface, and cement soil-soil interface. The

Table 2: Summary of pile test results.

No.	Maximum load (kN)	Maximum displacement (mm)	Ultimate load (kN)	Ultimate displacement (mm)
TP1	10000	73.5	8800	36.7
TP2	9600	81.9	8800	35.7
TP3	8000	24.0	>8000	—

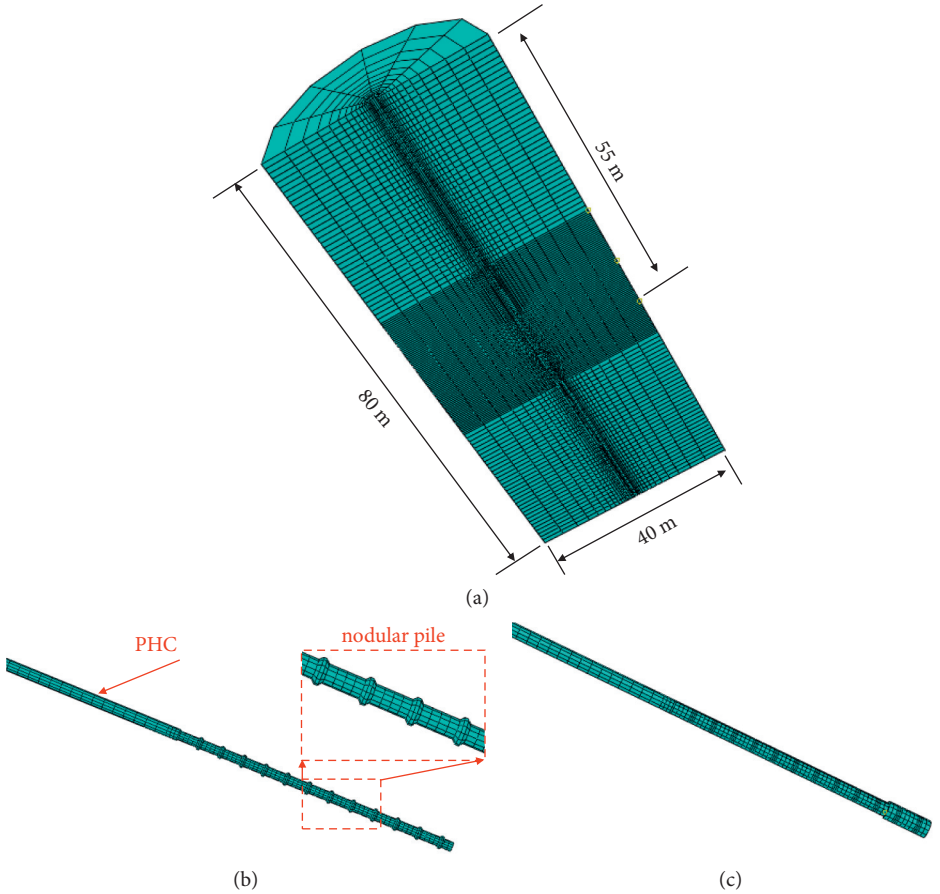

Figure 2: 3D finite element mesh. (a) Soil. (b) Precast pile. (c) Cement soil around the precast pile.

contact behavior of all three interfaces was defined using an isotropic Coulomb friction model, which allowed for slippage and separation between the master and slave surfaces. The feasibility and accuracy of using the Coulomb friction model to simulate the pile-soil interaction had been well verified by many researchers [16–18]. Their ultimate friction resistance is expressed as

$$\tau_{\text{crit}} = \min\left(\mu\sigma_y, \tau_{\max}\right), \tag{1}$$

where μ is the friction coefficient of the interface, σ_y is the normal stress, and $\tau_{\max}$ is the control value of ultimate friction, which was obtained by back analysis of the axial force of pile shaft in field test (as shown in Table 1).

To understand the characteristics of concrete-cement soil interface more clearly, the model tests were carried out using a cylindrical interface model device, as shown in Figure 4. The strength grade of concrete material was C40, and the volume ratio of cement grout and slurry was set to 0.15 and 0.6 in two groups. The test results showed that when the *UCS* of cement soil was 522~4572 kPa, the interfacial shear strength increased with the increase of *UCS*; the value was 0.167 to 0.224 (mean value 0.193). The *UCS* of cement soil of pile shaft was conservatively taken as 1.0~2.0 MPa. According to the results of this interface model test, it was conservatively estimated that the interface friction force provided by concrete-cement soil was 170~340 kPa. However, the ultimate local shaft resistance of cement soil-soil in PPEB pile in Shanghai was about 100 kPa [2]. Therefore, it could be seen that the friction performance of precast pile-cement soil interface was obviously better than that of cement soil-soil interface. Therefore, the friction coefficient of the precast pile-cemented soil interface was set to 0.80 to ensure high friction performance between precast pile and cement soil.

The friction coefficient (μ) of the pile-soil interface can be calculated by equations (2) and (3) [19]:

Figure 3: Sampling by the hanging bag method.

Table 3: Test results of cement soil at the enlarged base.

Soil	Water-cement ratio	Cement grout : slurry (volume ratio)	*UCS* (MPa)	E_{50} (MPa)	c (kPa)	φ (°)
Silty clay	0.6	1 : 1	6.22	862	—	—
	0.6	1.5 : 1	9.12	1149	857	43.9
	0.6	2 : 1	12.70	1745	—	—
Silty sand	0.6	1 : 1	11.60	901	—	—
	0.6	1.5 : 1	13.46	1496	1121	45.7
	0.6	2 : 1	17.02	2206	—	—

Table 4: Parameters of the precast pile and cement soil.

Pile material	c (kPa)	φ (°)	E (MPa)	v	Constitutive model
Precast pile	—	—	60000	0.15	Linear elastic
Cement soil around the precast pile	400	40	150	0.30	Mohr–Coulomb
Cement soil at the enlarged base	1000	45	1500	0.25	Mohr–Coulomb

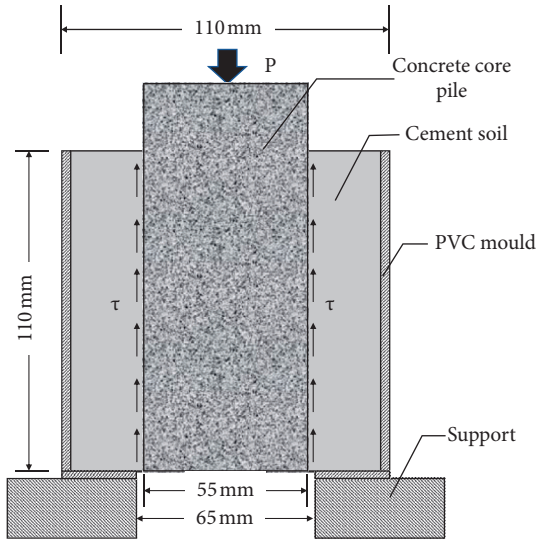

Figure 4: Schematic diagram of concrete-cement soil interface test.

$$\delta = \tan^{-1}\left(\frac{\sin\varphi\ \cos\varphi}{1+\sin^2\varphi}\right), \quad (2)$$

$$\mu = \tan\delta, \quad (3)$$

where φ is the friction angle of soil and δ is the internal friction angle of the pile-soil interface. When the friction angle φ is equal to 15° to 30°, the friction coefficient μ is equal to 0.23 to 0.35 from (2) and (3). The internal friction angle of the pile-soil interface can be also estimated according to (0.7~1.0) φ [20]. When $\varphi = 15\sim30°$, $\delta = 0.8\varphi$, the friction coefficient μ is equal to 0.21 to 0.45. Considering the field geological conditions, the friction coefficient between the precast pile and soil in the model was taken as 0.35.

Part of the cement soil slurry infiltrates into the soil around the PPEB pile, so the friction performance of the cement soil-soil interface is generally better than that of the concrete-soil interface. Combined with the results of the back analysis of the field test, the friction coefficient of the cement soil-soil interface was set to 0.53.

3.4. Validation of the Numerical Results. The load-displacement curve and axial force distribution of the test pile calculated by ABAQUS program are shown in Figure 5. The FEA modeling well simulated the bearing and deformation behavior of the field test pile, which showed that the established three-dimensional model and the selected parameters were reasonable. Therefore, based on this three-dimensional numerical model, it was reliable to analyze the main factors affecting the compressive bearing performance.

4. Compressive Bearing Characteristics of the PPEB Pile

4.1. Analysis of Compressive Bearing Characteristics. The development of the plastic zone of the PPEB pile-soil system during loading is shown in Figure 6. AC YIELD is the yield mark [21], which is equal to 1 when yielding occurs and 0 in the case of unyielding. Since the value of the node is determined by interpolation, it may be more than 1 or less than 0 when displayed, but it does not affect the reliability of the calculation results. The representative loading conditions of the test pile are also shown in Figure 6, in which Q_1 is the elastic limit load, Q_3 is the ultimate load, Q_2 is the intermediate transition load, and Q_4 is the maximum load.

Before the initial loading stage Q_1, the shaft resistance of PPEB pile in the upper soil was gradually mobilized; at the same time, the toe resistance had also played a role and increased with the loading. After loading Q_2, the soil at the outer edge of the enlarged base was the first to enter the plastic state; there was a trend of separation between the shoulder of the enlarged base and the soil, so the stress relaxation of the soil led to yield. As the loading continued, the shaft resistance reached the limit, and more loads would be borne by the soil around the enlarged base. The plastic zone of the soil at the outer edge of the enlarged base gradually expanded and ran through the bottom of the enlarged base. When loaded to the ultimate load Q_3, the soil stress relaxation zone whose length was about 1 time the diameter of the enlarged base was formed above the variable cross section of the enlarged base. After the ultimate load Q_3, the continued loading was mainly borne by the soil at the end of the pile, and the plastic zone developed to the upper part of soil. The cement soil under the last nodule of the nodular pile also formed a yield zone due to the increase of stress and gradually developed from the bottom to the top of the enlarged base. Finally, the PPEB pile reached the maximum load Q_4. During the whole loading process, there was no plastic zone in the cement soil around the pile shaft, which indicated that the strength of cement soil could ensure the bond strength of the interface between the precast pile and the cement soil.

4.2. Stress Analysis of the Pile Shaft. The comparison between the total axial force of PPEB pile and the axial force of the precast pile under representative loading conditions is shown in Figure 7. For the nonenlarged base part, the stiffness of the cement soil around the pile was lower, so the axial force of the PPEB pile was mainly controlled by the precast pile. As the property of the cement soil at the enlarged base was much better than that around the precast pile, the load sharing of the enlarged base could not be ignored. $\triangle Q$ in Figure 7 is the load shared by the cement soil in the PPEB pile. The axial force of the cement soil at the enlarged base increased sharply with the depth and reached the maximum below the last nodule. On the contrary, the axial force of the precast pile decreased sharply within the range of the enlarged base. This reflected the role of the enlarged base. The force was transferred to the cement soil of the enlarged base through the nodules and then to the soil around the enlarged base. It was the reaction of a larger range of soils that enhanced the end bearing capacity of the PPEB pile. Under the ultimate load Q_3, the enlarged base resistance (axial force of 52 m section) accounted for about 26% of the applied load, which was close to the field test results [5]. Under the loading of Q_1, Q_2, Q_3, and Q_4, the toe resistance (axial force of 55 m section) was 830, 965, 1415, and 2765 kN, respectively, accounting for 14%, 13%, 16%, and 27% of the total load.

The stress of the cement soil was much less than that of the precast pile, so that the load was first transferred from the precast pile to the cement soil and then to the soil around the pile. The vertical stress of cement soil in the upper pipe pile increased gradually along the depth. The vertical stress distribution of the lower nodular pile section was more complex. In the process of loading, each nodule was squeezed with its lower cement soil and had a tension trend with the upper cement soil. Therefore, within the range of each nodule, the vertical stress of the cement soil under the nodule was the largest, while the vertical stress of the cement soil above the next nodule was the smallest.

The vertical stress of the cement soil of the enlarged base was also clearly different above and below each nodule, as shown in Figure 8. The vertical stress of the cement soil

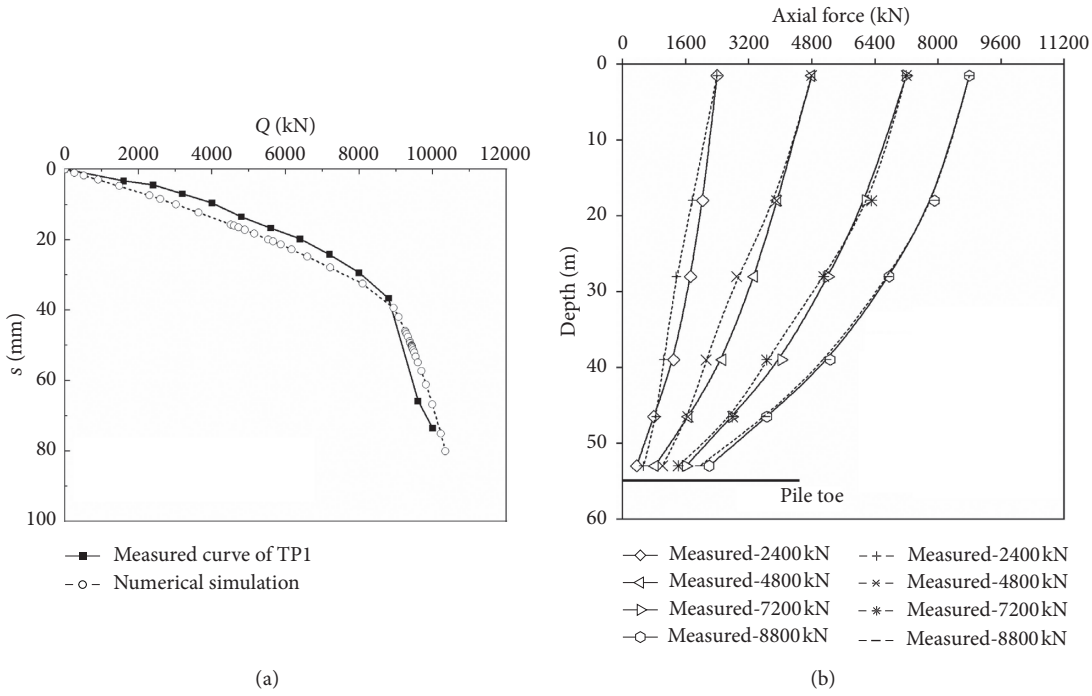

Figure 5: Comparison between FEA and measured values. (a) Q-s curve. (b) Axial force of the PPEB pile.

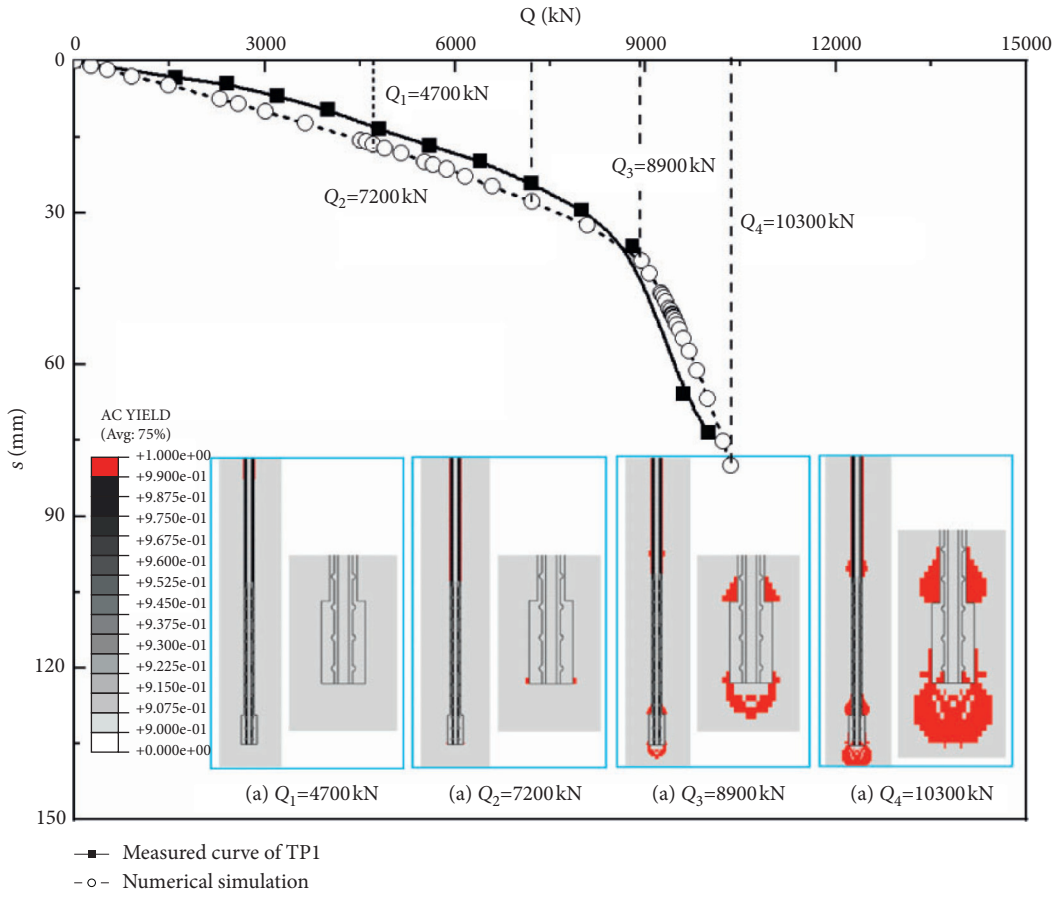

Figure 6: The development process of the yield zone around the pile and the enlarged base.

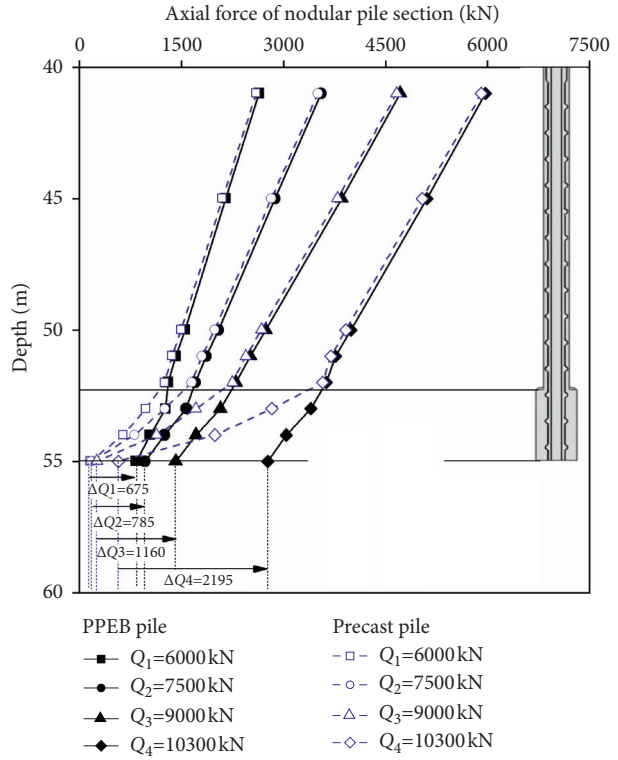

Figure 7: Axial force distribution of the nodular pile section.

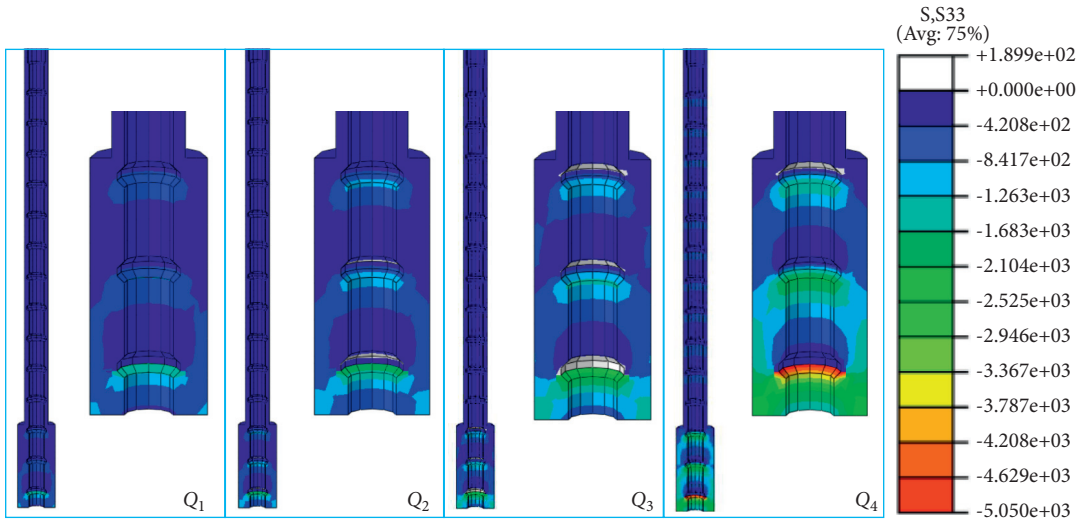

Figure 8: Vertical stress change of cement soil at the enlarged base during loading.

under the last nodule was the largest and developed upward. After the elastic load Q_1, the tensile stress zone occurred above the last nodule. With the ultimate load Q3 applied, the tensile stress zone appeared above the three nodules in the enlarged base. After Q_3, the extrusion of nodules was strengthened. However, the extrusion deformation was restricted by the displacement of the pile toe; the tensile stress zone was gradually closed from bottom to top.

The cement soil of the enlarged base was also subjected to a higher shear stress. Figure 9 shows that, under the ultimate load Q_3, the shear stress (1260 kPa) of the cement soil under the last nodule was obviously higher than that of the soil at the end of the pile (265 kPa). Therefore, when the strength of the cement soil was not enough, the compression failure or shear failure of the cement soil might occur before the soil failure at the end of the pile.

5. Parameter Analysis

Horizontally, the structure of the PPEB pile is nonuniform, and longitudinally the size of the pile shaft is different (with enlarged base), as shown in Figure 10, so there are many

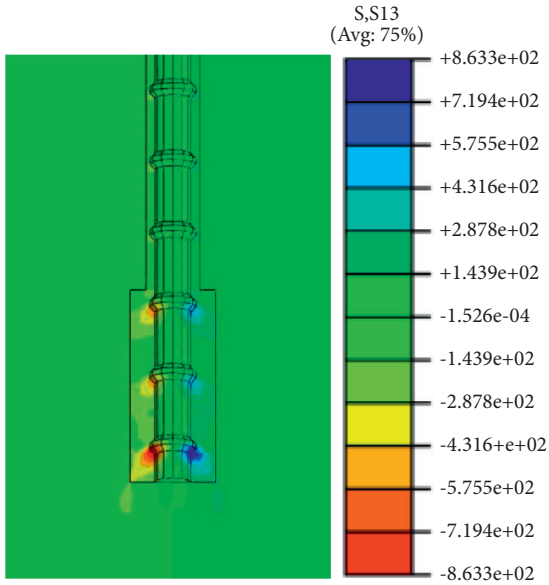

Figure 9: Shear stress distribution of cement soil at the enlarged base and surrounding soil (Q_3).

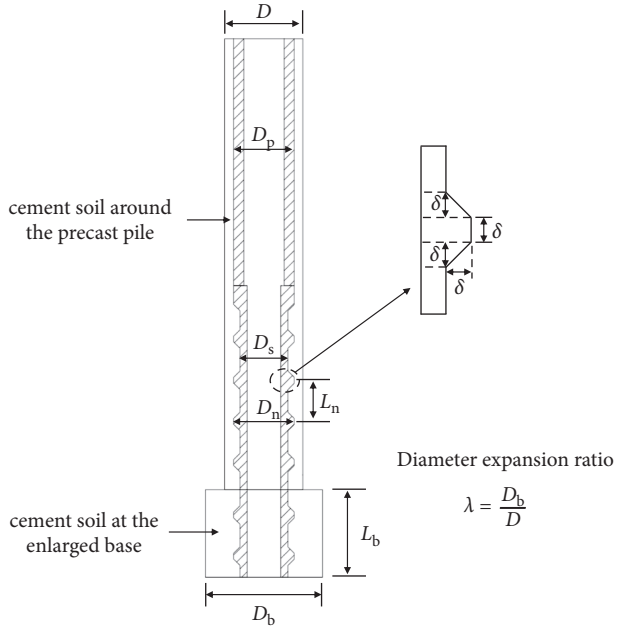

Figure 10: Schematic diagram of the pile structure of the PPEB pile.

factors affecting its bearing performance. Based on the three-dimensional FEA model established above, the influencing factors such as the height and diameter of the enlarged base, proportion of the nodular pile, spacing of the neighboring nodules, and thickness of cement soil were analyzed.

5.1. The Height of the Enlarged Base. The setting of the enlarged base is an important feature that distinguishes the PPEB piles from other bored precast piles and concrete-cored deep cement mixing piles. The structure of the enlarged base has a great influence on the bearing performance. In the modeling calculation, the height of the enlarged base (L_b) was taken as 0, 1.0, 2.0, 2.7, 4, and 5 m, respectively (i.e., 0D, 1.3D, 2.7D, 3.6D, 5.3D, and 6.7D; D is the diameter of borehole), including 0, 1, 2, 3, 4, and 5 nodules, respectively.

The calculation results are shown in Figure 11. Combined with the characteristics of *Q-s* curve and the development of soil plastic zone, the ultimate bearing capacity was defined, as shown in Figure 11(a). Comparative analysis of the ultimate bearing capacity of PPEB piles under different enlarged base heights is shown in Figure 11(b). Based on the case without enlarged base ($L_b = 0$), when $L_b = 1.3$D, 2.7D, 3.6D, 5.3D, 6.7D, the ultimate bearing capacity increased by 11.7%, 13.0%, 13.9%, 15.5%, and 16.7%, respectively. It could be shown that the existence of the enlarged base (i.e., including one nodule) could dramatically improve the bearing capacity, but with the increase of the height of the enlarged base, the increase of bearing capacity was limited. Therefore, in actual projects, the height of the enlarged base is 3 times the borehole diameter, which contains 2~3 nodules, and the force of the enlarged base can be guaranteed.

5.2. The Diameter Expansion Ratio of the Enlarged Base. The diameter expansion ratio (λ) was defined as the ratio of the enlarged base diameter to the borehole diameter. In the modeling calculation, the diameter expansion ratio λ was set to 1.0, 1.3, 1.6, and 2.0, and the end bearing layer was set to medium-dense silt mixed silty clay (⑦) and dense silty sand (⑧).

The numerical results under different conditions of diameter expansion ratio and pile end bearing layer are shown in Figure 12. The better the end bearing layer was, the greater the ultimate bearing capacity was. Similarly, the larger the diameter expansion ratio was, the greater the ultimate bearing capacity was; in addition, the proportion of toe resistance increased linearly. The choice of expansion ratio is more controlled by whether the strength of the enlarged base meets the requirements of punching or compression resistance and the limitation of the construction equipment capacity. In practical engineering, the diameter expansion ratio is generally controlled at 1.6.

5.3. Proportion of the Nodular Pile. PHC nodular pile is generally used in the lower part of PPEB pile, and the nodules can effectively enhance the bonding force between the precast pile and cement soil. Especially at the end of the pile shaft, the PHC nodular pile and the enlarged base form a whole and bear the load together. In the numerical model, the length of the nodular pile segment was set to 0, 4, 15, 28, 40, and 55 m from the pile toe, accounting for 0%, 7%, 27%, 50%, 73%, and 100% of the total pile length, respectively.

With the proportion of nodular piles increased from 7% to 100%, the pile head displacement increased significantly while the ultimate bearing capacity increased only by about 3.5%, as shown in Figure 13. Since the stiffness of the nodular piles was smaller than that of PHC piles with the same diameter, the deformation increased with the increase of the proportion of nodular piles under

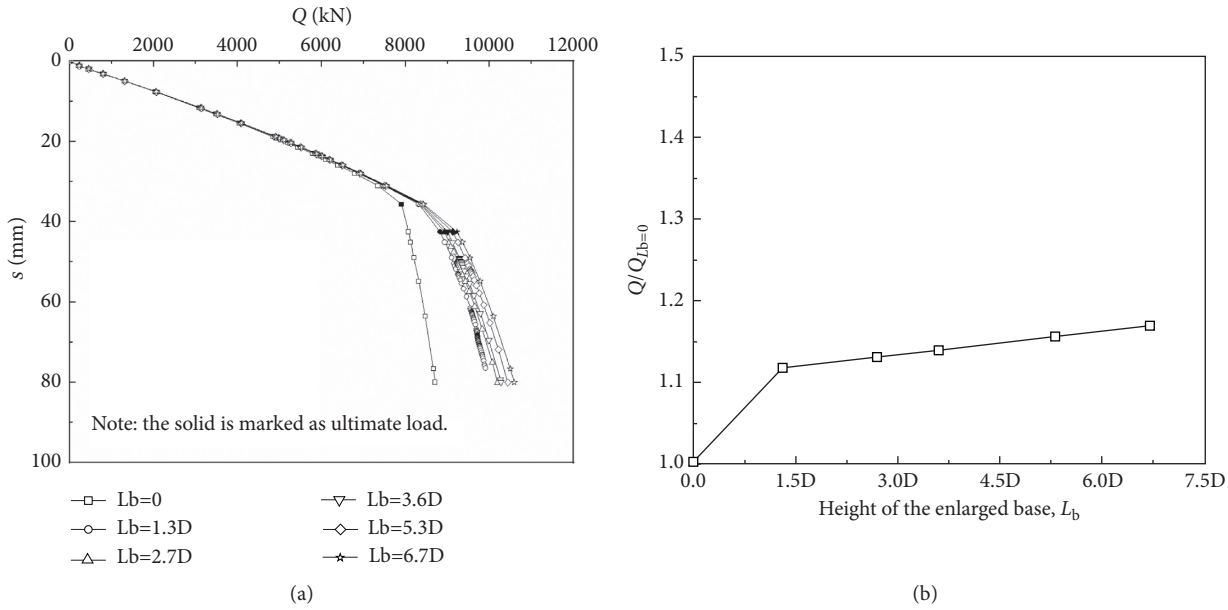

Figure 11: Influence of the height of the enlarged base on bearing capacity. (a) *Q-s* curves. (b) Comparison and analysis.

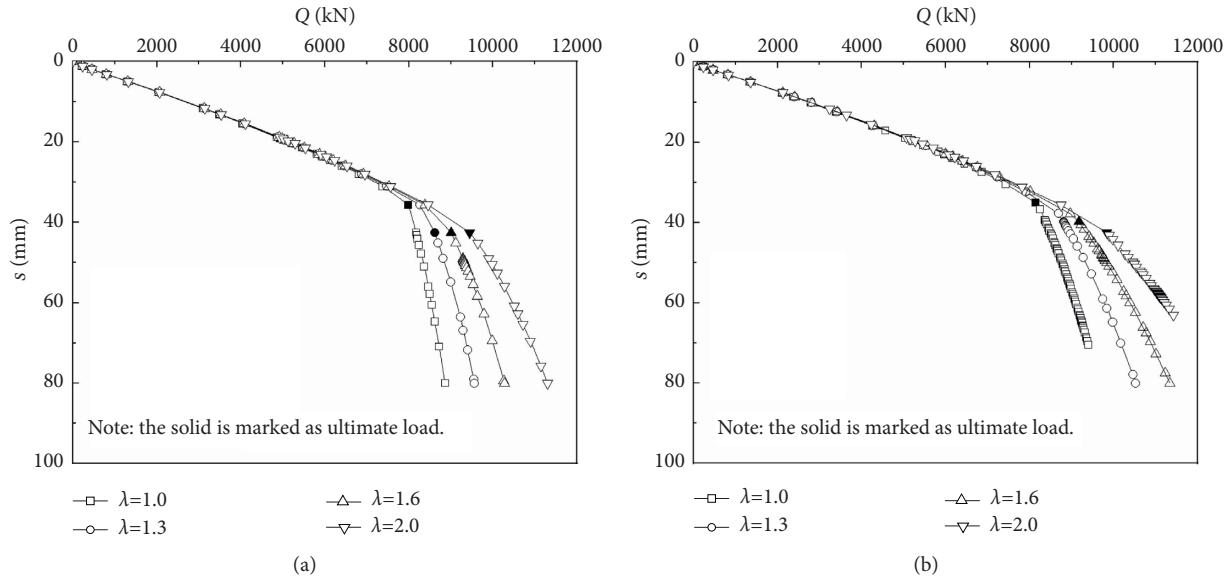

Figure 12: Influence of the expansion ratio of the enlarged base and bearing layer. (a) End bearing layer, ⑦ silt mixed silty clay. (b) End bearing layer, ⑧ silty sand.

the same loads. In particular, the PHC nodular pile used in the upper part of the pile shaft (such as 100%) was subject to a large load, which would share a larger pile deformation. On the other hand, the larger pile head displacement led to the larger pile-soil relative displacement, which improved shaft resistance to a certain extent. Therefore, in projects with high requirements for deformation, it is a more reasonable form to set up 1 ~2 section nodular piles in the lower part of the PPEB pile.

5.4. Spacing of the Neighboring Nodules. The spacing of the neighboring nodules (L_n) of nodular piles was set to 1, 2, 3, and 4 m for analysis. Under the condition of cement soil ($UCS = 1.7 \sim 4.0$ MPa) of the field test piles, the load-displacement curves were almost the same when using the above different spacing, as shown in Figure 14. The curves showed that the change of spacing of the neighboring nodules from 1 m to 4 m had no obvious effect on the bearing capacity. There might be two main reasons for this result. First, the cement soil around the precast pile had good properties, which could ensure the high bond strength of the interface between the precast pile and the cement soil; high interface strength resisted the relative displacement between nodular pile and cement soil, thus weakening the influence of nodules and spacing of the

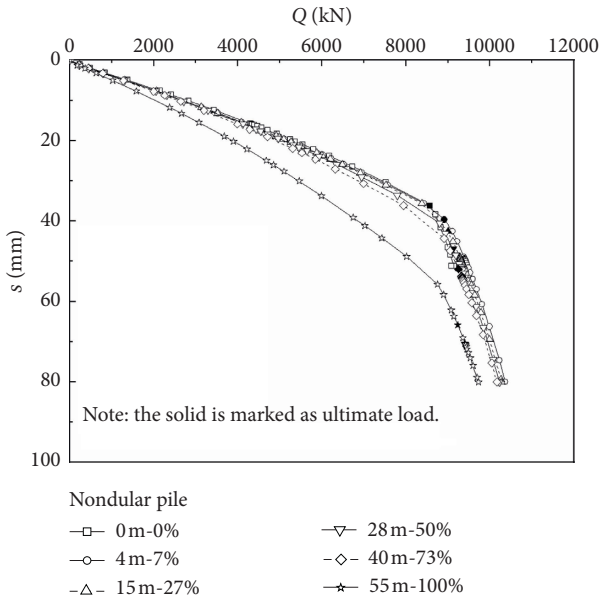

Figure 13: Influence of the proportion of the nodular pile on bearing capacity.

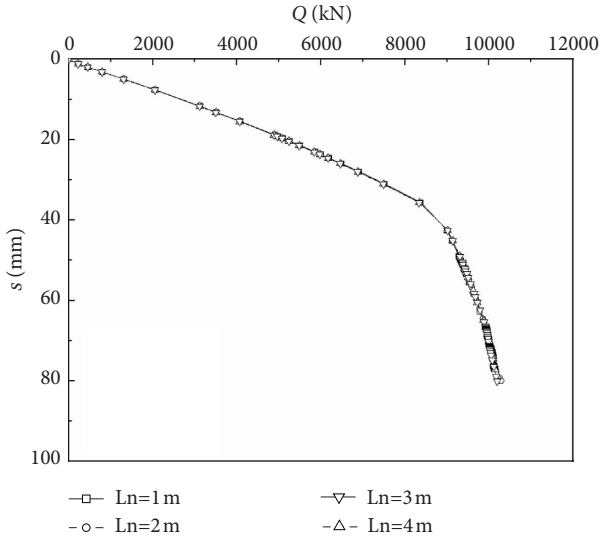

Figure 14: Influence of the spacing of the neighboring nodules on bearing capacity.

neighboring nodules on the bearing performance. Second, in the numerical model, the nodular piles were in the lower part and accounted for only 27% of the pile length, so that the overall influence of the nodular pile segment was not significant. Hence, when the property of cement soil around the precast pile is good and the proportion of nodular piles is relatively small, the 1 m spacing commonly used in the project can be optimized.

5.5. Thickness of Cement Soil. The thickness of cement soil in PPEB pile varies with the diameter of the borehole. In the FEA model, the 650 mm (500 mm) diameter nodular pile was used in the lower part. When the diameter of cement soil borehole (D) was set to 750, 850, 950, and 1050 mm, the thickness of cement soil was 125, 175, 225, and 275 mm, respectively, in nonnodules.

Under the condition that the size of the enlarged base was constant, the bearing capacity increased nonlinearly with the increase of the thickness of cement soil, as shown in Figure 15(a). The efficiency analysis was based on the borehole diameter of 750 mm of the test pile, as shown in Figure 15(b). Although the increase of shaft resistance was similar to the development of bearing capacity, the increase rate of shaft resistance per unit area continued to decrease. It can be inferred that, for deep soft soil areas, the efficiency of improving the bearing capacity by increasing the thickness of cement soil is low.

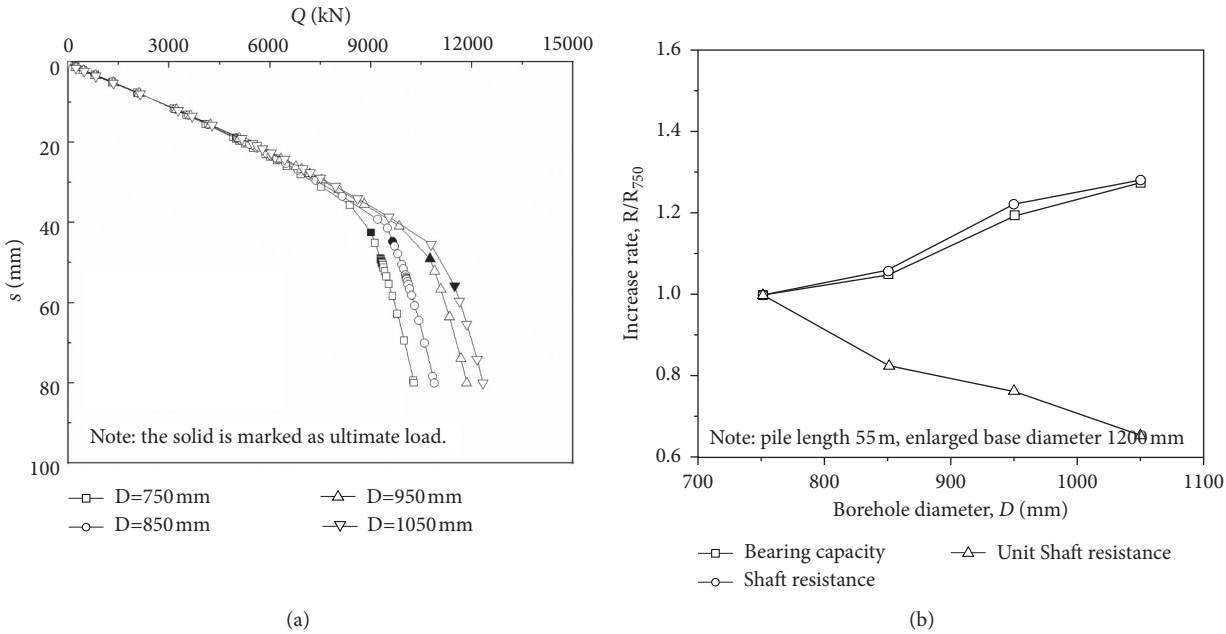

Figure 15: Influence of the thickness of cement soil (diameter of the borehole) on bearing capacity. (a) Comparison of bearing capacity. (b) Efficiency analysis.

6. Conclusions

Based on the static load test and key parameters test in deep soft soil in Shanghai, a three-dimensional FEA model was established using ABAQUS. Then, the bearing characteristics of the PPEB pile were analyzed. The main conclusions are as follows:

(1) The Mohr–Coulomb elastic-plastic model was adopted for the cement soil around the pile shaft and at the enlarged base, and the elastic modulus was 150 MPa and 1500 MPa, respectively. The friction coefficients of precast pile-cement soil interface and cement soil-soil interface were 0.80 and 0.53, respectively. The numerical results well simulated the bearing and deformation behavior of the field test pile.

(2) At the initial stage of loading, the load had been transferred to the pile toe, and with the increase of the applied load, the shaft resistance was gradually mobilized from top to bottom. In the nonenlarged base part, the axial force of the PPEB pile was mainly controlled by the precast pile. In the enlarged base part, the load was transferred to the cement soil of the enlarged base through nodules and then to the soil around the enlarged base. The cement soil of the enlarged base was subject to higher vertical compressive stress and shear stress.

(3) The existence of an enlarged base could greatly improve the compressive bearing capacity of the PPEB pile. Increasing the diameter and height of the enlarged base was beneficial to the bearing capacity, and the effect of diameter expansion ratio was more effective. In practical engineering, it is reliable to control the enlarged base diameter at 1.6 times the borehole diameter and adopt the enlarged base height of 3 times the borehole diameter.

(4) With the increase of the proportion of nodular piles, the ultimate bearing capacity increased slightly, and the deformation increased obviously. Setting up 1 ~2 section nodular piles in the lower part of the PPEB pile is a more reasonable measure for projects with higher deformation requirements. When the property of cement soil around the precast pile is good and the proportion of nodular piles is relatively small, the 1 m spacing commonly used in projects can be optimized.

(5) The bearing capacity increased nonlinearly with the increase of the thickness of cement soil. For deep soft soil areas, the efficiency of improving bearing capacity by increasing the thickness of cement soil is low.

Data Availability

The data used to support this study are available from the corresponding author upon request.

Conflicts of Interest

The authors declare that they have no conflicts of interest.

Acknowledgments

This study was supported by the Program of Shanghai Academic/Technology Research Leader (no. 18XD1422600), the China Postdoctoral Science Foundation (no. 2021M690784), and the Science and Technology Plan of

Guangzhou Municipal Construction Group (no. 2020-KJ013).

References

[1] R. H. Zhang, L. L. Wu, and Q. H. Kong, "Research and practice of JZGZ pile foundation," *Chinese Journal of Geotechnical Engineering*, vol. 35, no. S2, pp. 1200–1203, 2013.

[2] Z. Ling, W. Wang, J. Wu, M. Huang, and J. Yuan, "Shaft resistance of pre-bored precast piles in Shanghai clay," *Proceedings of the Institution of Civil Engineers - Geotechnical Engineering*, vol. 172, no. 3, pp. 228–242, 2019.

[3] J.-J. Zhou, X.-N. Gong, K.-H. Wang, and R.-H. Zhang, "Shaft capacity of the pre-bored grouted planted pile in dense sand," *Acta Geotechnica*, vol. 13, no. 5, pp. 1227–1239, 2018.

[4] J. Zhou, X. Gong, and R. Zhang, "Model tests comparing the behavior of pre-bored grouted planted piles and a wished-in-place concrete pile in dense sand," *Soils and Foundations*, vol. 59, no. 1, pp. 84–96, 2019.

[5] W. D. Wang, Z. Ling, J. B. Wu, and J. Yuan, "Field study on bearing characteristics of pre-bored precast pile with enlarged base in Shanghai," *Journal of Building Structures*, vol. 40, no. 2, pp. 238–245, 2019.

[6] W. D. Wang, Z. Ling, and J. B. Wu, "Experimental study on pile-forming effect and quality of pre-bored precast pile with enlarged base in Shanghai area," *Building Structure*, vol. 49, no. 12, pp. 115–119, 2019.

[7] G. Ye, Y. Cai, and Z. Zhang, "Numerical study on load transfer effect of Stiffened Deep Mixed column-supported embankment over soft soil," *KSCE Journal of Civil Engineering*, vol. 21, no. 3, pp. 703–714, 2017.

[8] A. Wonglert and P. Jongpradist, "Impact of reinforced core on performance and failure behavior of stiffened deep cement mixing piles," *Computers and Geotechnics*, vol. 69, pp. 93–104, 2015.

[9] C. Phutthananon, P. Jongpradist, P. Yensri, and P. Jamsawang, "Dependence of ultimate bearing capacity and failure behavior of T-shaped deep cement mixing piles on enlarged cap shape and pile strength," *Computers and Geotechnics*, vol. 97, pp. 27–41, 2018.

[10] M. Yang, Z. M. Zhang, and N. W. Liu, "Numerical simulation of compressive mechanical characters of new bored grouting PHC nodular pile," *Rock and Soil Mechanics*, vol. 34, no. 7, pp. 2119–2126, 2013.

[11] J.-J. Zhou, X.-N. Gong, K.-H. Wang, R.-H. Zhang, and J.-J. Yan, "Testing and modeling the behavior of pre-bored grouting planted piles under compression and tension," *Acta Geotechnica*, vol. 12, no. 5, pp. 1061–1075, 2017.

[12] C. Xie, "Numerical study on behaviors of the pre-bored grouting planted nodular pile under compression and tension," MS Thesis, Zhejiang University, Hangzhou, China, 2018.

[13] China Academy of Building Research, *JGJ 106-2014 Technical Code for Testing of Building Foundation Piles*, China Architecture & Building Press, Beijing, China, 2014.

[14] M. Yang and X. H. Zhao, "Analysis of single pile in layered soil," *Journal of Tongji University*, vol. 20, no. 4, pp. 421–427, 1992.

[15] A. M. Grzyb-Faddoul, *Numerical analysis of the reinforcement of existing foundations by the soil mixing technique*, PhD Thesis, Lyon:Institut National des Sciences Appliquées (INSA), Villeurbanne, France, 2014.

[16] A. V. Rose, R. N. Taylor, and M. H. El Naggar, "Numerical modelling of perimeter pile groups in clay," *Canadian Geotechnical Journal*, vol. 50, no. 3, pp. 250–258, 2013.

[17] Y. Khodair and A. Abdel-Mohti, "Numerical analysis of pile-soil interaction under axial and lateral loads," *International Journal of Concrete Structures and Materials*, vol. 8, no. 3, pp. 239–249, 2014.

[18] A. Wang, D. Zhang, and Y. Deng, "Lateral response of single piles in cement-improved soil: numerical and theoretical investigation," *Computers and Geotechnics*, vol. 102, pp. 164–178, 2018.

[19] M. F. Randolph and C. P. Wroth, "Application of the failure state in undrained simple shear to the shaft capacity of driven piles," *Géotechnique*, vol. 31, no. 1, pp. 143–157, 1981.

[20] J. G. Potyondy, "Skin friction between various soils and construction materials," *Géotechnique*, vol. 11, no. 4, pp. 339–353, 1961.

[21] Abaqus, *Analysis User's Manual, Version 6.14*, Dassault Systemes Simulia Corp, Johnston, RI, USA, 2014.